

Hilbert-Huang transform analysis of surface wavefield under tropical cyclone Hudhud

Sourav Mandal*, M. Anjali Nair, V Sanil Kumar

Ocean Engineering Division, CSIR-National Institute of Oceanography,
Goa, 403004, India

*Corresponding author e-mail address: sourav@nio.org

Abstract

The characteristics of an evolving ocean surface wavefield under tropical cyclone Hudhud that took place in October 2014 are investigated. The Hilbert-Huang transformation (HHT) is used for the spectral analysis of the cyclone generated waves. Empirical mode decomposition (EMD) is used to decompose the wave data into different intrinsic mode function (IMF). Hilbert Marginal Spectra and the Fourier Spectra for the wavefield data and the corresponding IMF are compared. In addition to the frequency wave elevation spectrum, the wave group characteristics and their relationship with the local wave characteristics are studied.

Keywords: Hilbert-Huang transform, Empirical mode decomposition, Spectral analysis, Wave group, tropical cyclone.

1. Introduction

The Bay of Bengal is one of the largest semi-enclosed basins and is the region where the deadliest tropical cyclones occurred ([1]). A tropical cyclone (TC) with intense and fast-varying winds produces a severe and complex ocean wave field that can propagate thousands of kilometers away from the storm center, resulting in dramatic variation of the wave field in space and time ([2]). Tropical cyclone-generated wave fields are of interest both for understanding the wave characteristics and for predicting potentially hazardous conditions for ship navigation and coastal regions. A number of studies were carried out to understand wave generation and wave growth during Hurricane ([3 4,5, 6, 7, 8, 9, 10]). In the Bay of Bengal, the largest significant wave height (H_s) measured is 8.4 m on 28 October 1999 during the passage of Orissa super cyclone ([11]). During the TC Phailin, a maximum significant wave height of 7.3 m and a maximum wave height of 13.5 m is measured at 50 m water depth off Gopalpur on 12 October 2013 ([10]).

A cyclonic storm Hudhud originated from a low-pressure system that formed under the influence of an upper air cyclonic circulation in the Andaman Sea on 6 October 2014 intensified into a cyclonic storm on 8 October 2014 and as a severe cyclonic storm on 9 October 2014. Severe Cyclonic Storm Hudhud made landfall about 30 km west-northwest of Visakhapatnam (Northern Andhra Pradesh state, India) on 12 October, noon local time. The maximum sustained wind speeds were 115 knots (Joint Typhoon Warning Center), corresponding to a weak Category 4 hurricane on the Saffir-Simpson Hurricane Wind Scale. The east coast of India is subject to infrequent severe cyclones and Hudhud represents the strongest storm since a late October/early November storm of 1998, which included sustained winds to 140 knots.

The spectral analysis is used in the analysis of wave time series data in the form of spectral functions. While Fourier analysis is widely accepted as one of the most useful tools in spectral data analysis, many researchers found that it is not suitably applicable for the analysis of nonlinear and nonstationary data series due to nonlinearity and periodicity issue (see [12, 13, 14, 15]). However, recently Singh et al. [16], demonstrated Fourier analysis's applicability for the decomposition of nonlinear and non-stationary time series. It is well known that during the storm, the wave characteristics become highly non-linear during TC. However, in the past, several studies are conducted to detect non-linearity and non-stationarity of a time series. Choudhury et al. [17] applied a higher-order statistical method to detect non-linearity based on the oscillations source under the assumption of stationary data. Elsayed [18] studied the phase coupling and non-linear between wind wave and ocean wave by wavelet-based bicoherence method. Later, Dong et al. [19] and Ma et al.

[20] used wavelet-based bicoherence method to study non-linear interactions in laboratory-generated waves. On the other hand, Fourier-based bicoherence also used by many (see [21, 22, 23]) to study non-linear interactions in ocean waves. An excellent review of different non-stationary data processing methods is done by Huang et al. [13] and they proposed the Hilbert-Huang transform (HHT) method to deal with a given non-linear and non-stationary time series. HHT method is applied to measure non-linearity and non-stationarity of a signal by computing stationarity and linearity index (see [24, 25, 26]). The HHT method is used to decompose a given signal into a finite number of Intrinsic Mode Functions (IMF) using Empirical Mode Decomposition (EMD). From these IMFs, the local energy and the instantaneous frequency, which represents the intrinsic oscillatory modes embedded in the given signal can be derived. Later, by adding adaptive noise, the EMD algorithm is improved by ensemble empirical mode decomposition (EEMD) algorithm (see [27]) and complete ensemble empirical mode decomposition (CEEMD) algorithm (see [28]). The application of HHT method in non-linear water waves is also studied [29, 30]. HHT method gives a very sharp time resolution for the energy-frequency content of the signal, which is important in order to study wave group structure under different sea states.

In the past, several studies have been done to understand the wave group structure. Goda [31] examined simulated wave profiles and introduced group run length to study wave groupiness. Based on the local wavelet energy density, a new non-dimensional groupiness factor is introduced and studied the wave group structure of mechanically generated irregular waves using that groupiness factor [32]. A detailed review of the methodologies commonly used for wave group analysis is also carried out [33, 34]. Liu [35] used the wavelet transform to investigate individual wave groups, characterized by time group length and group energy. However, in the last two decades, several authors have used the HHT method to study the wave records and wave group structure under different sea states. The concept of instantaneous frequency was used for the investigation of the group structure and the transformation of wave groupiness from deep to shallow water [36]. Schlurmann [37] investigated the application of the HHT in spectral analysis of non-linear water waves generated in a laboratory wave flume and of the waves from the Sea of Japan. Veltcheva and Soares [38] used HHT to examine the contribution of different IMFs associated with the wave data collected off the Portuguese coast. Ortega et al. [39] studied the North Sea storm and investigated the number of IMFs and energy associated with them. Recently, the abnormal wave group characteristics is studied by wave envelope-phase and HHT method [40].

In the present study, the data measured during 1-20 October 2014 is analysed to study the surface wave characteristics during TC Hudhud. The spectral analysis of the data is carried out using the

HHT method and the results compared with the classical Fourier method. The energy distribution among different IMFs is studied. The wave group structure is analyzed using time group length and group energy during different sea stages.

2. Field data

In connection with the real-time wave data collection program, a Datawell Directional Waverider buoy was moored at 15-m water depth (latitude: $17^{\circ} 37.94'$ N longitude: $83^{\circ} 15.66'$ E) off Gangavaram, south of Visakhapatnam (Fig. 1) and the data collection was ongoing since February 2010. The data measured during 1-20 October 2014 are analysed to study the surface wave characteristics during TC Hudhud. The time referred to in the paper is Coordinated Universal Time (UTC) and the local time is Indian Standard Time (IST), which is 5:30 h ahead of UTC. Wave data are recorded continuously at 1.28 Hz, and heave is measured in the range of -20 to 20 m with a resolution of 1 cm and an accuracy of 3%. The details of the buoy used for wave measurement, wave data analysis and the wave characteristics of the study area are presented by Anjali Nair et al. [41].

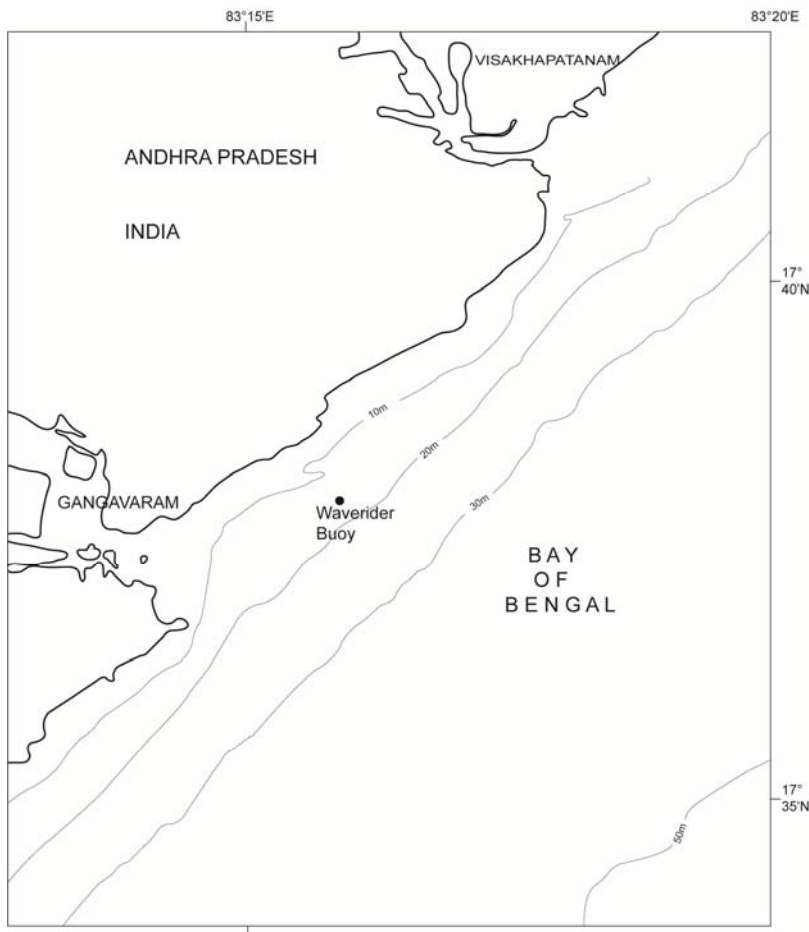


Figure 1. Study area along with the buoy location

3. Methodology

The detailed procedure of the HHT method and its performance over several Fourier based method for time-frequency distribution of energy can be found in [13, 40, 42]. HHT method mainly decomposes a non-stationary and non-linear time series into different Intrinsic mode functions (IMF) using an empirical method called the Empirical Mode Decomposition (EMD). Then instantaneous frequency, amplitude and energy can be obtained and presented as a Hilbert spectrum. In order to avoid inconsistencies in the definition of the instantaneous frequency, IMFs must satisfy two conditions: i) the number of local extreme points and of zero-crossings must either be equal or differ at most by one and ii) at any point, the mean of the envelopes defined by the local maxima and minima must be zero. If $X(t)$ is an original signal then $X(t) = \sum_{j=1}^r C_j(t) + d_{r+1}$, where

$C_j(t)$ ($j=1,2,\dots,r$) is IMF and $d_{r+1}(t)$ is referred as residual. After decomposition of the signal into different IMFs, Hilbert transformation is applied to different IMFs, which is given by,

$$H_j(t) = \frac{1}{\pi} \int_{-\infty}^{\infty} \frac{C_j(\tau)}{t - \tau} d\tau, \text{ where the integral is given by Cauchy principal value. Now, if } Z_j(t) \text{ is}$$

the analytical signal associated with, $Z_j(t) = C_j(t) + iH_j(t) = A_j(t)e^{i\theta_j(t)}$, where the amplitude function $A_j(t) = \sqrt{C_j(t)^2 + H_j(t)^2}$ and phase function $\theta_j(t) = \arctan[H_j(t)/C_j(t)]$. Hence, the

instantaneous frequency can be expressed as $\omega_j(t) = \frac{d\theta_j(t)}{dt}$. Thus the original signal $X(t)$

can be expressed as

$$X(t) = \text{Re} \left[\sum_{j=1}^n A_j(t) \exp\left(i \int \omega_j(t) dt\right) \right].$$

The time-frequency distribution of the amplitude function is defined as the Hilbert amplitude spectrum and the time-frequency distribution of the squared amplitude function is defined as the Hilbert energy spectrum. However, in the present study, Hilbert energy spectrum is considered as Hilbert spectrum $H(\omega, t)$. The marginal spectrum

$$h(\omega) = \int_0^T H(\omega, t) dt, \text{ where } T \text{ is the total time duration of the wave record. The Marginal Hilbert}$$

Spectrum shows the total energy contributed by each frequency value. The instantaneous energy $IE(t)$ can be obtained as, $IE(t) = \int_w H^2(\omega, t) d\omega$.

4. Results and discussion

4.1 Wave characteristics

The wave height started to increase on 9 October 2014 at 0930 hrs from 0.7 m and reached 7.5 m on 12 October 2014 at 1030 hrs due to the cyclone (Fig. 2a). The average H_s during 7-8 October 2014 is 0.73 m and increased to 4.3 m on 12 October 2014. The increase in T_{m02} before the arrival of the cyclone indicates that the swells generated by the cyclone reached the location before the cyclone (Fig. 2b). The peak wave period reduced from 13-15 s to 9-12 s during the cyclone (Fig. 2c). The wave direction before the arrival of the cyclone is from 160 to 180° and during the cyclone, the wave direction changed to 110 to 130° (Fig. 2d). The time series plots containing the high waves on 12 October 2014 are presented in Figure 3. The height of the waves before and after the maximum wave height measured is 55 to 84% of the maximum value. The maximum wave height measured is 10.75 m and the second-highest wave in the same 30 minutes record is 10.2 m (Fig. 3). H_s for the 30 minutes record containing the highest waves is 7.5 and the ratio of H_{max} to H_s is ~ 1.4 and is lower than the theoretical value of 1.62 to 1.64 for 190 to 220 waves ([44]).

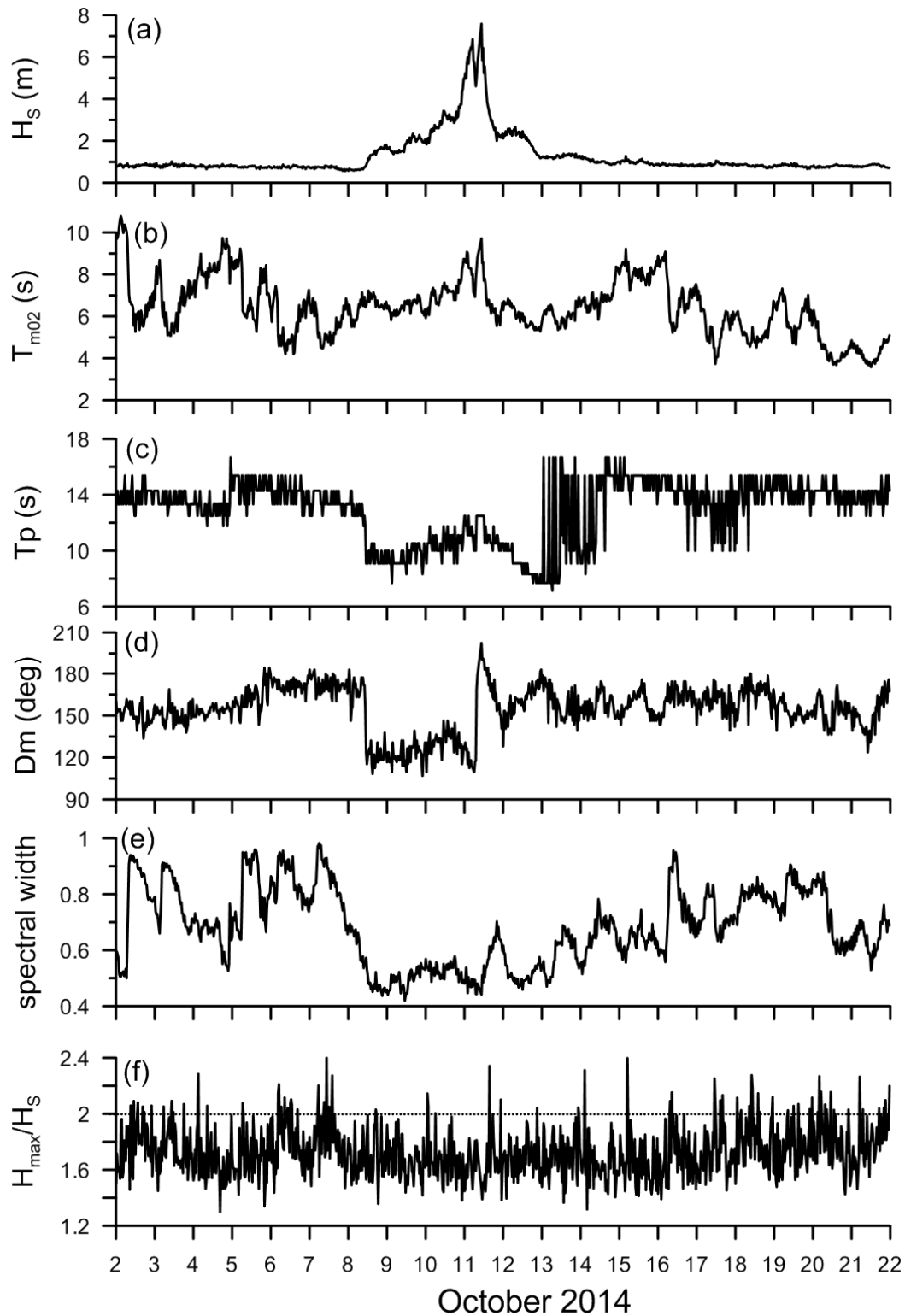


Figure 2. Variation of a) significant wave height, b) mean wave period, c) peak wave period, d) mean wave direction, e) spectral width parameter and f) ratio of maximum wave height to significant wave height from 2 to 22 October 2014.

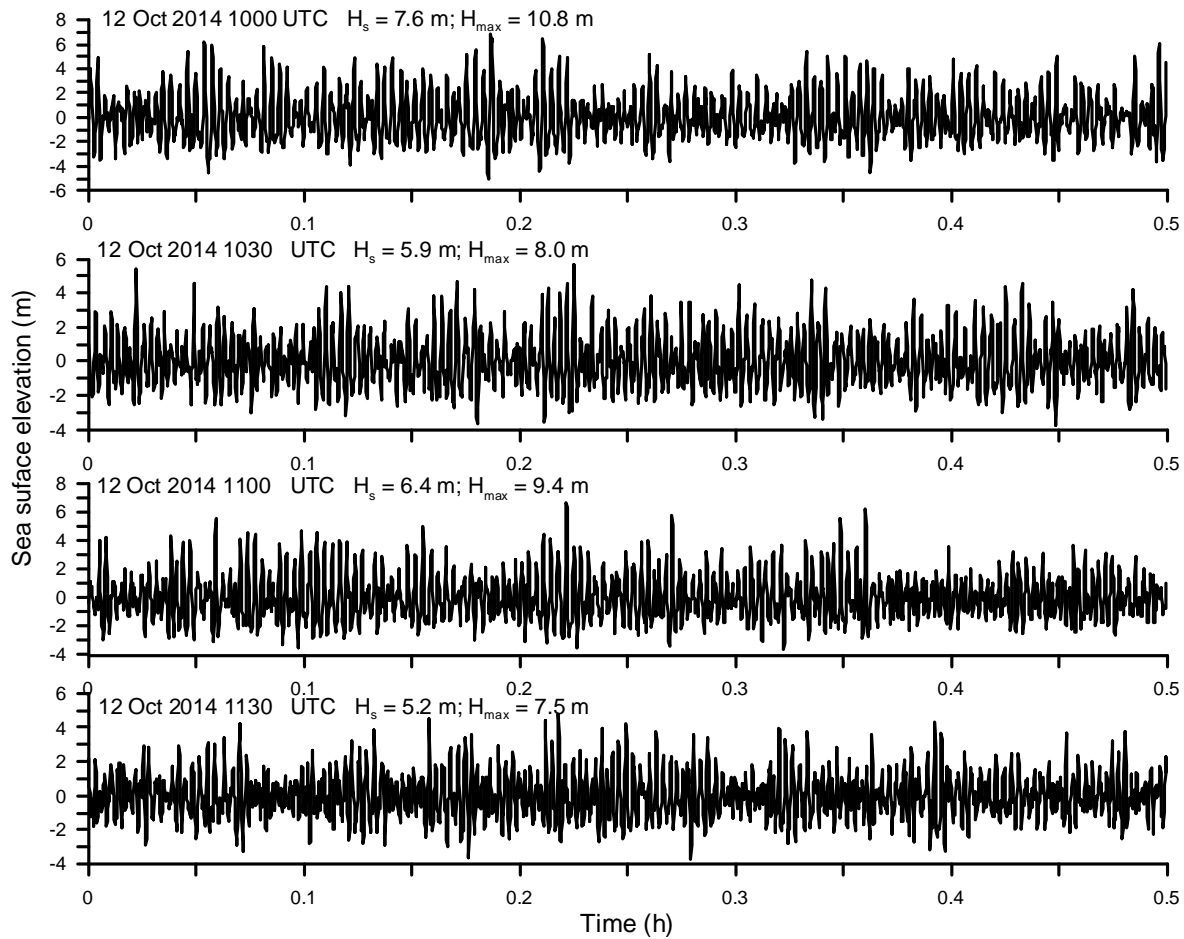


Figure 3. Time series plot of the sea surface elevation for 0.5 h on 12 October 2014 at different times

During the cyclone, the ratio between H_{\max} and H_s for the 30 minutes record varied from 1.4 to 2.3 with an average value of 1.66 (Fig. 2f) and the average value measured is close to the theoretical value. From 11 to 12 October 2014, freak waves, wave with abnormality index (H_{\max}/H_s) > 2, are observed four times (Fig. 2f). The freak waves are featured by a single and steep crest causing severe damage to structures and ships ([45]). Since the wave data during the cyclone has a peak period between 9.1 and 12.5 s with an average value of 10.8 s, the available sea states are in a regime of intermediate and shallow water depth. Under these circumstances, the Rayleigh distribution shows a discrepancy with the measured data (Fig. 4). The presence of wind-sea and swell simultaneously affect the non-linear dynamics and in turn, the short-term statistics. For the record with 100 to 1000 waves, the ratio of H_{\max} to H_s is within a 10% deviation from the theoretical Rayleigh distribution (Fig. 5).

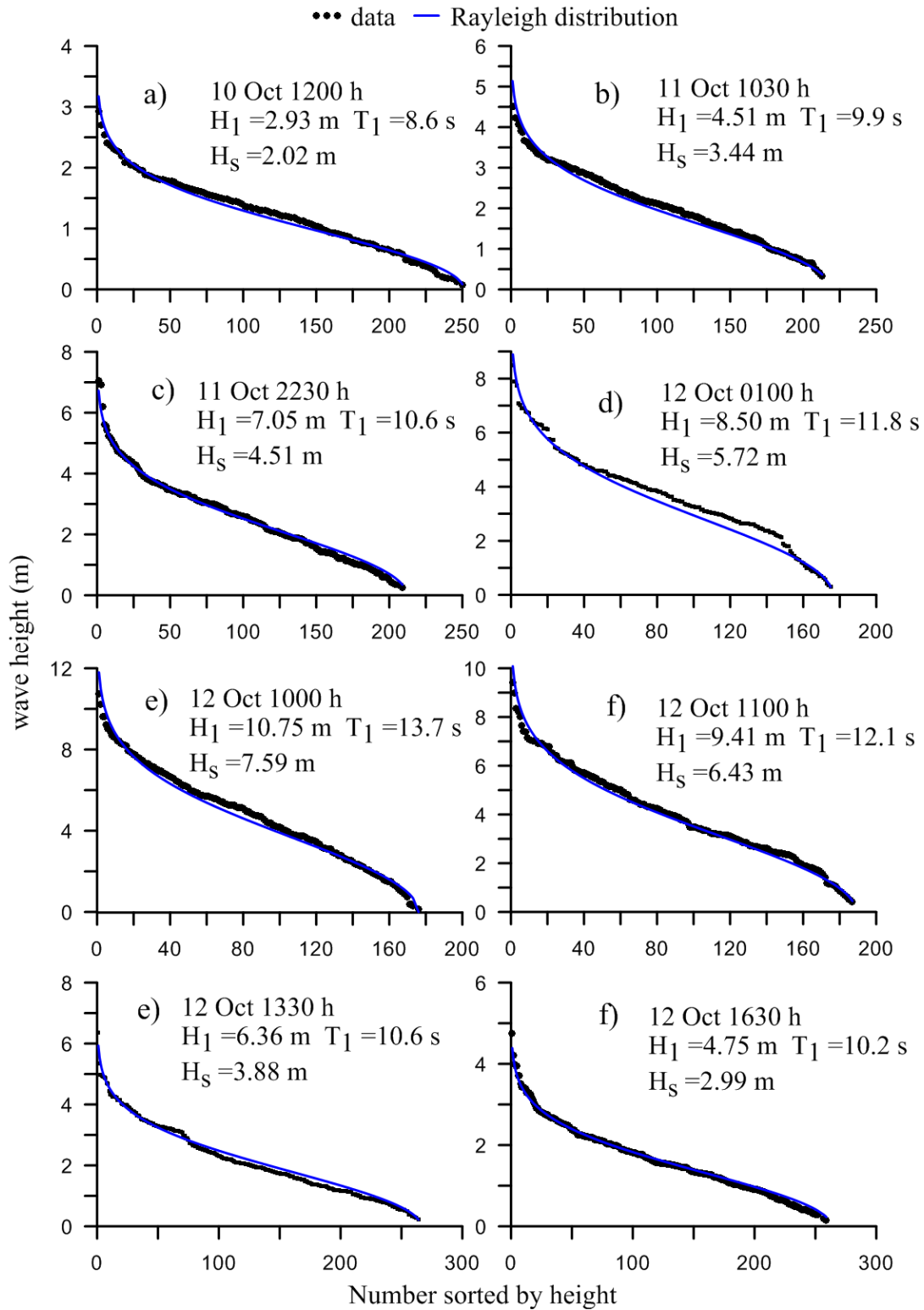


Figure 4. Plot of wave height measured and estimated using Rayleigh distribution during 30 minutes for selected time.

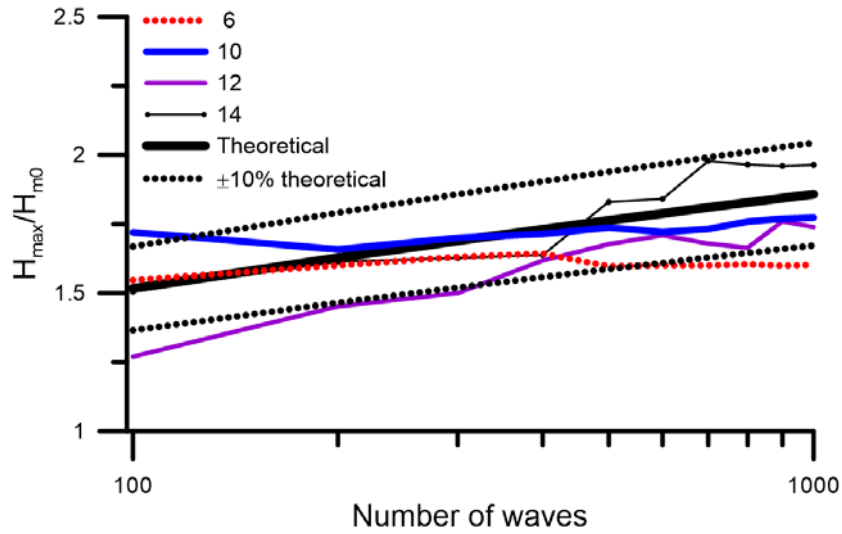


Figure 5. Ratio of H_{\max} and H_s for record with number of waves 100 to 1000 in different days. The ratio of H_{\max} and H_{m0} based on Rayleigh distribution is also shown in black thick line along with 10% variation (dotted black line).

Since there is a large variation in the spectral energy density during and before the cyclone, the normalized spectral energy density is plotted to indicate the shift in the peak frequency during the cyclone (Fig. 6a). During the cyclone, the peak frequency shifted from lower (0.06 to 0.08 Hz) to higher frequencies (0.09 to 0.14 Hz) due to the increase in the locally generated waves. Before and after the cyclone, the peak frequency is around 0.06 to 0.08 Hz. It is important to note that, during the evolution of TC Hudhud, JONSWAP and Donelan spectrums are used to fit the double-peaked spectrum. JONSWAP handles the first peak while the Donelan spectrum is used to fit second peak. However, for some single peaked spectrum, for higher frequency range, Donelan spectrum is used for fitting. During the growing stage of TC, JONSWAP is used for spectrum fitting, while during fully developed stage (single peak) and decaying stage (double peak), both JONSWAP and Donelan spectrum are used. The spectrum is narrow-banded (peakedness parameter > 2) during growing and fully developed stages but broad-banded during the decaying stages. The slope of the high-frequency tail of the spectrum changes between -4.13 and -2.92 during the TC. More details of spectral characteristics of TC Hudhud can be found in Anjali Nair and Sanil Kumar [46]. Amrutha et al. [10] observed that the skewness, the degree of vertical asymmetry of the surface elevation vary with the directional width. As the directional width reduces, the skewness increases indicating that at high sea states, the sea surface elevation is positively skewed and the directional spreading of spectral energy density is minimum [10]. On 10 October 2014, the skewness values are less than 0.15 and on 12

October 2014, the skewness increased to 0.5. The average directional width is 24.5° and 21° on 10 October and 12 October 2014 (Fig. 6c).

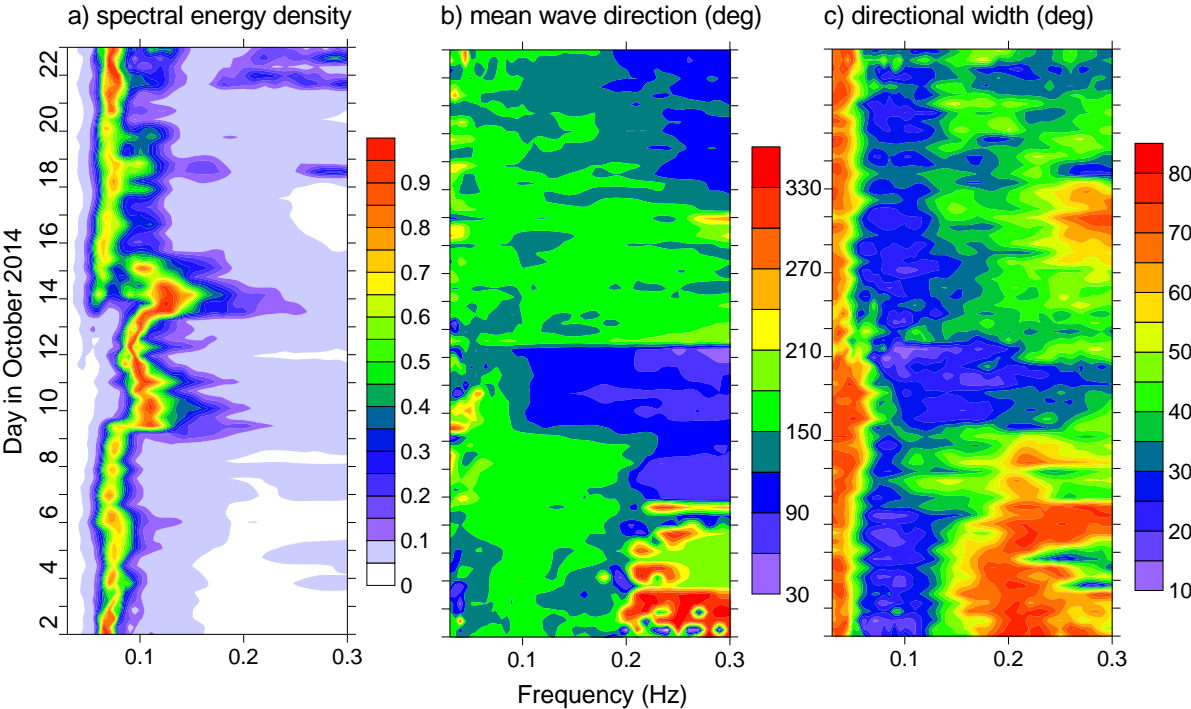


Figure 6. Time history of (a) normalised spectral energy density, (b) mean wave direction and (c) directional width with frequency during 2 to 22 October 2014

4.2 Hilbert spectrum

The measured wave data sets are decomposed into various time scales components as a set of IMFs using the EMD process described in Section 3. However, the number of IMF obtained for each record is not the same (Table 1).

Table 1. Variance of different IMFs for D1-D8.

IMF No.	Var. %	Cum %	IMF No.	Var. %	Cum %	IMF No.	Var. %	Cum %	IMF No.	Var. %	Cum %
10 Oct 1200 UTC (D1)			11 Oct 1030 UTC (D2)			11 Oct 2230 UTC (D3)			12 Oct 0100 UTC (D4)		
2	56.84	56.84	2	74.44	74.44	2	79.19	79.19	2	70.59	70.59
1	31.69	88.53	3	12.21	86.66	3	9.91	89.11	3	15.05	85.65
3	9.93	98.46	1	11.05	97.71	1	8.16	97.28	1	11.76	97.42
4	0.8	99.26	4	1.46	99.18	4	1.79	99.07	4	1.42	98.84
5	0.36	99.62	5	0.46	99.64	5	0.45	99.52	5	0.64	99.48
6	0.18	99.8	6	0.14	99.79	7	0.27	99.79	10	0.22	99.70
7	0.13	99.9	8	0.09	99.88	6	0.16	99.96	7	0.12	99.83
8	0.07	100	9	0.06	99.95	8	0.03	99.99	6	0.10	99.93
9	0	100	7	0.04	100	9	0.00	100	9	0.06	99.99
									8	0.00	100
12 Oct 1000 UTC (D5)			12 Oct 1100 UTC (D6)			12 Oct 1330 UTC (D7)			12 Oct 1630 UTC (D8)		
2	59.21	59.21	2	68.74	68.74	2	61.03	61.03	2	62.15	62.15
1	28.37	87.59	1	19.95	88.69	1	24.13	85.17	3	17.88	80.04
3	10.35	97.95	3	9.39	98.09	3	12.28	97.45	1	16.87	96.92
5	0.74	98.69	4	1.24	99.33	4	1.37	98.83	4	2.11	99.04
4	0.68	99.38	5	0.33	99.67	5	0.45	99.29	6	0.36	99.41
6	0.44	99.83	7	0.09	99.76	7	0.21	99.50	5	0.34	99.76
7	0.15	99.98	6	0.07	99.84	6	0.21	99.71	7	0.15	99.91
8	0.01	100	8	0.07	99.92	9	0.16	99.88	8	0.07	99.98
			10	0.04	99.96	8	0.11	100	9	0.01	100
			9	0.03	100						

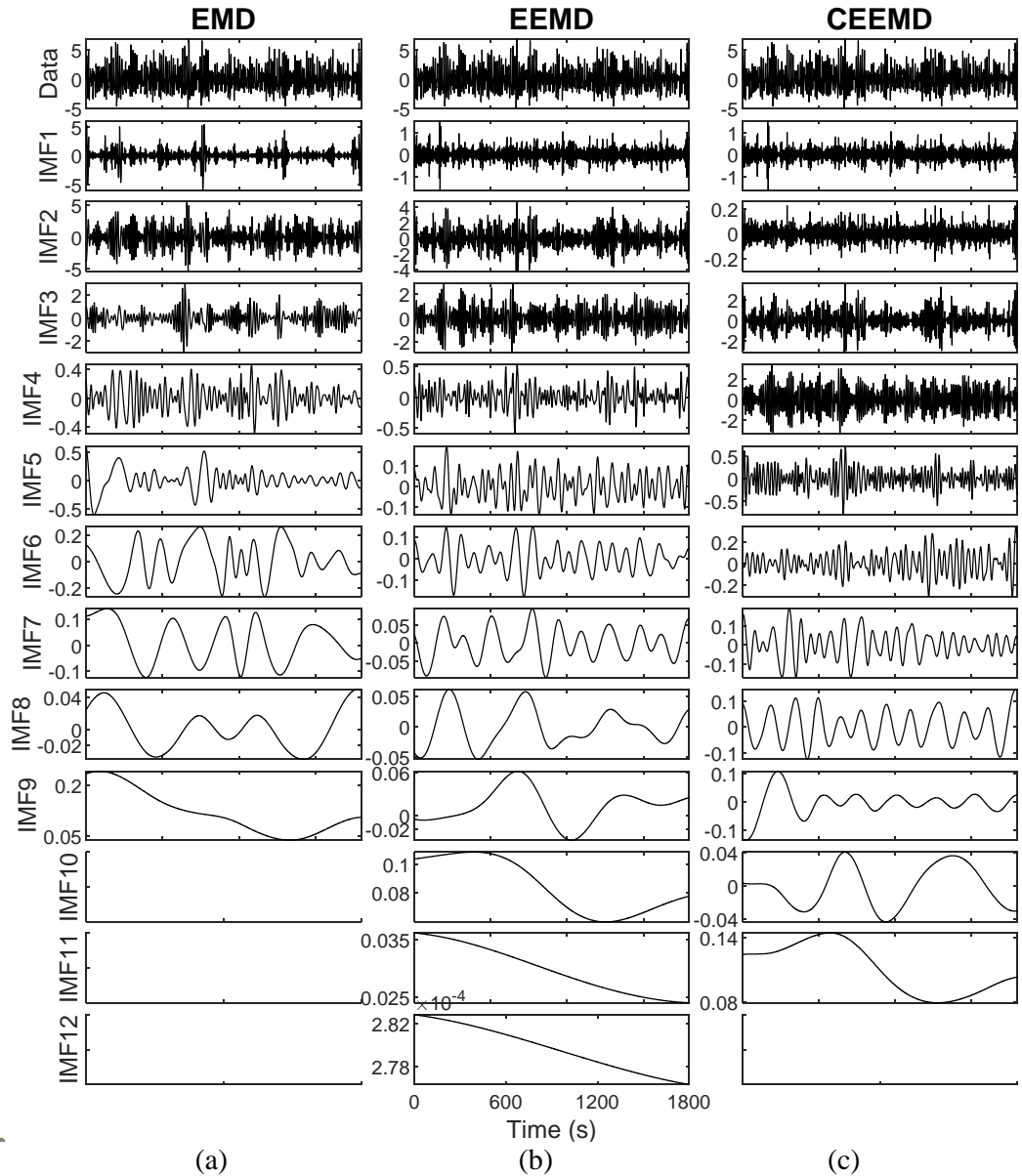


Figure 7. Decomposition of original wave record of D5 by (a) EMD, (b) EEMD and (c) CEEMD.

According to the basis of significant wave height observed in different wave records during 10-12 October, eight wave measurements (D1-D8, see Table 1) are selected for analysis. These 8 observations are classified into four different sea states, namely calm (D1), wave growth (D2-D4), wave decay (D5-D6) and post-storm (D7-D8).

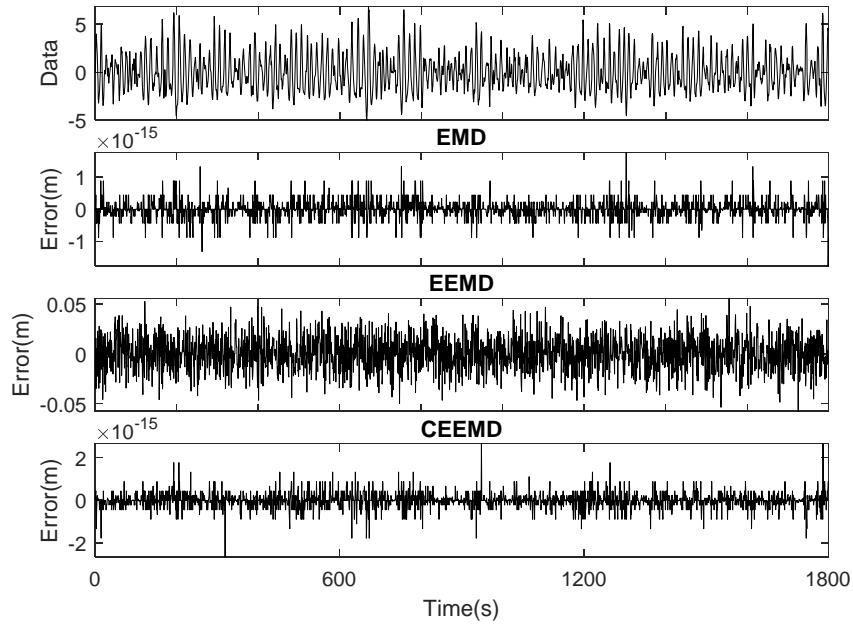


Figure 8. Difference between the original wave record of D5 and sum of its IMFs and residue by EMD, EEMD and CEEMD.

In figure 7, original wave data D5 recorded at 15m water depth is decomposed by (a) EMD, (b) EEMD and (c) CEEMD method. An ensemble size of 500 and standard deviation 0.2 are used in EEMD and CEEMD. The last component of Figure 7 is residue, which is a trend. It can be observed that EEMD provides higher number of IMFs compare to EMD and CEEMD. The EMD, EEMD and CEEMD methods yield 8, 11 and 10 IMFs of D5 respectively. The mean period of each IMFs can be derived from the mean value of instant frequency. These IMFs represents a different range of energy. This can be seen in Figure 10(a). In case of EMD, it can be observed that IMF2 is most dominant, while IMF 2 and IMF 4 are most dominant in the cases of EEMD and CEEMD. Dominant IMF carries most of the energy of the original wave record. To show the completeness of EMD, EEMD and CEEMD numerically, the difference between reconstructed wave data by adding all the IMFs components of D5 and original wave record D5, Figure 8(a) is plotted. In case of EMD, the maximum amplitude of error is less than 2×10^{-15} while in case of CEEMD, the maximum amplitude of error is less than 1×10^{-15} . On the other hand, EEMD does not guarantee the complete decomposition.

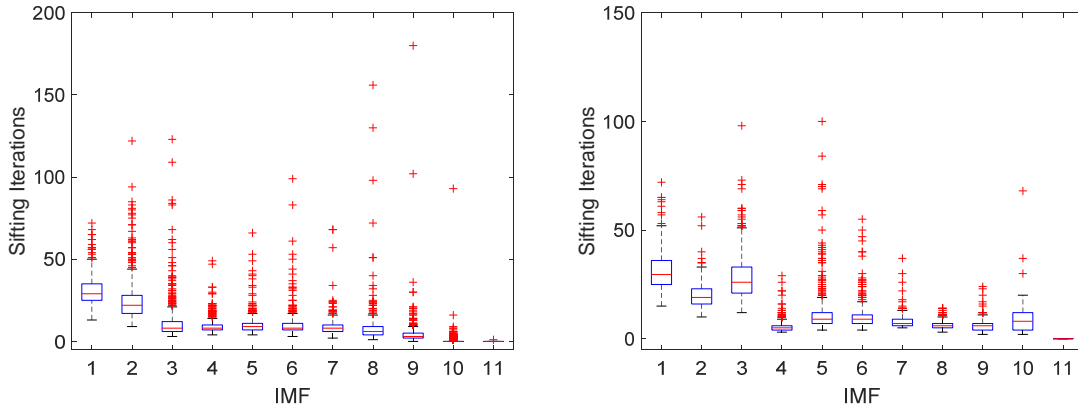


Figure 9. Sifting iterations vs different IMFs for (a) EEMD and (b) CEEMD. In figure 9, boxplots of the sifting iterations for different IMF are shown for (a) EEMD and (b) CEEMD. It is observed that the range of sifting iterations for EEMD is almost double of the sifting iterations of CEEMD. Hence, the computational cost for the CEEMD is lesser than for the EEMD case.

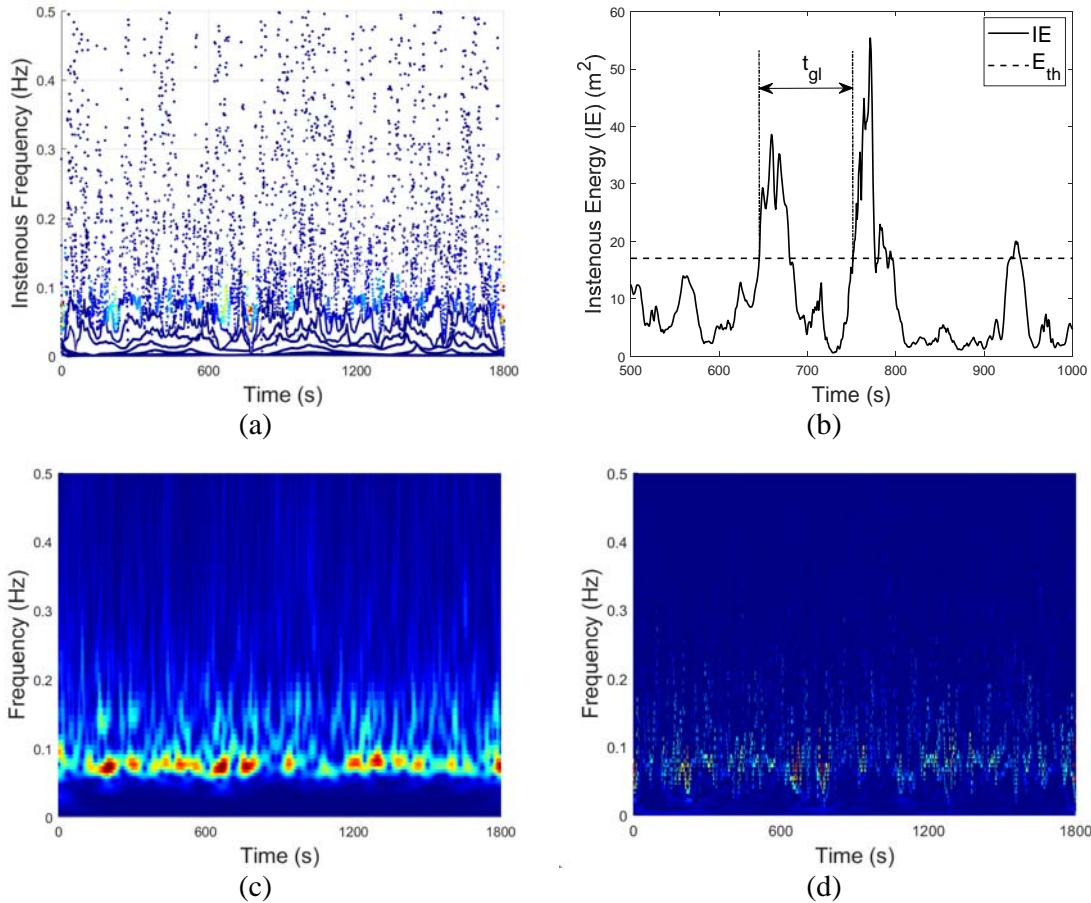


Figure 10. (a) Instantaneous energy spectrum, (b) a selected section of corresponding instantaneous energy, (c) Wavelet spectrum and (d) Hilbert spectrum for D5.

In Figure 10(a), the instantaneous energy spectrum is plotted for the wave record D5. The energy density skeleton can be observed in the figure. The figure reveals detailed variations of frequency, energy with time. It can be observed that most of the energy concentrated between the frequencies 0.03 Hz to 0.1 Hz. Most of the energy described by the IMF 1-3, which is shown in the Table 1. It is important to note that in the instantaneous energy, the wave is characterized within a narrow range of frequency, while in the Fourier spectrum, typical super-harmonic components can be observed. In Figure 10(b), the variations of instantaneous energy (IE) of a selected portion of the wave record D5 is shown. The concept of instantaneous energy (IE) is used here to determine the individual wave group. It is important to note that Instantaneous energy (IE) captures the time variation of wave energy without any filtration. Time group length and associated group energy is used here to characterize individual wave group as in [36]. To decide time group length, the threshold energy level (E_{th}) is taken as the mean value of the one-third of the highest instantaneous energy. The time group length (t_{gl}) is the time gap between two successive upcrossing of the threshold energy level by the instantaneous energy, as in Figure 10(b). The group energy (E_{gr}) is the total energy in that time group length, which can be expressed as $E_{gr} = \int_{t_{gl}} IE(t)dt$. It is found that for all the wave records D1-D8, threshold energy level (E_{th}) increases or decreases with the increase or decrease of significant wave height. In Table 1, the variance percentage shared by each IMF component and its cumulative percentage are shown. The table reveals that most of the energy (more than 96% of the total energy) of the wave record is captured by four IMFs (1-4). IMF 2 captures more than 50% of the total variance. For the selected 9 wave records D1-9, the maximum number of IMFs is found is 10, which is less compare to [39]. However, present observation on most energetic IMFs agrees with [47]. It can be observed that the wave record D5 with significant wave height 7.59 m, has the lowest number of IMFs, which is in contrast to [25]. It is important to note that during the cyclone, most of the wave energy contributed by the wind. Hence physically, most energetic IMFs may represent wind waves whilst less energetic IMFs may represent small ripples and lower frequency oscillations in the original wave record. In Figures 10(c) and (d), the Wavelet spectrum and Hilbert spectrum are compared. Wave energy is directly proportional to the square of the wave amplitude. From both of the figures, it is observed that the energy is concentrated between the frequencies 0.03 Hz to 0.1 Hz. In the case of Hilbert spectrum, each skeleton line represents each IMF while skeleton lines are not visible in the case of Wavelet spectrum. In Wavelet spectrum, amplitude contours are smoothed line. To smooth Hilbert spectrum, weighted spatial filter can be applied with large enough spatial averaging ([13]). However, smoothing will degrade time and frequency resolution of the Hilbert

spectrum. Original Hilbert spectrum has higher time and frequency resolution than Wavelet spectrum. Hence, for the physical interpretation, Hilbert spectrum serves better than the Wavelet spectrum.

4.3 Stationarity

To check the stationarity of the wave record, following ([13]), degree of stationarity (DS) and degree of statistical stationarity (DSS) are found out in this section. This index can give a quantitative measure of the non-stationarity of the whole wave record. The degree of stationarity can be expressed

as $DS(\omega) = \frac{1}{T} \int_0^T \left(1 - \frac{H(\omega, t)}{n(\omega)} \right)^2 dt$, where mean marginal spectrum $n(\omega) = \frac{1}{T} h(\omega)$. In Figure 11, the

degree of stationarity for the whole record of D5. is plotted in solid line. When the index value zero, the physical process becomes stationary. Hence, high index value shows high non-stationarity in the data. The figure reveals that the wave record D5, is highly non-stationary especially for the higher frequency component. To check the piecewise stationarity, the degree of statistical stationarity is found out. The degree of statistical stationarity can be expressed as

$DSS(\omega, \Delta t) = \frac{1}{T} \int_0^T \left(1 - \frac{\overline{H(\omega, t)}}{n(\omega)} \right)^2 dt$, where Δt is the short span of time (time steps), referred as time

window and $\frac{\overline{H(\omega, t)}}{n(\omega)}$ is the average value of $\frac{H(\omega, t)}{n(\omega)}$ over Δt .

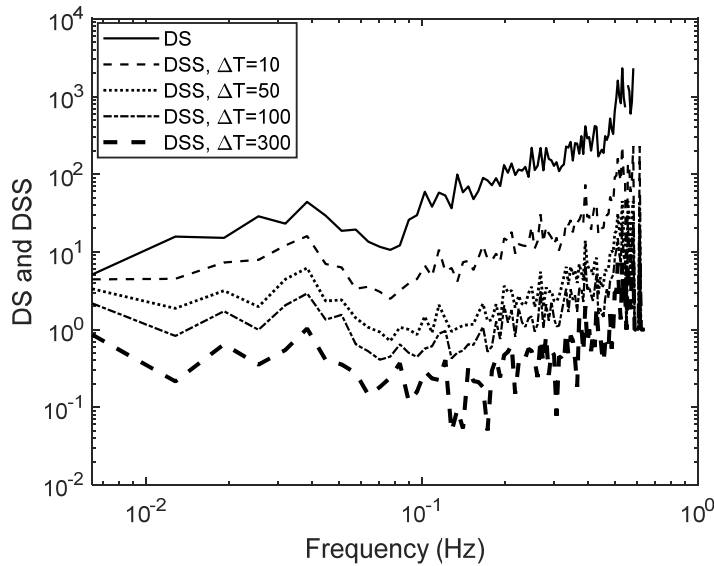


Figure 11. The variations of Degree of Stationarity (DS) and Degree of Statistical Stationarity (DSS) with frequency for wave record D5. DSS is plotted for different time window with Δt steps.

In Figure 11, to check the piecewise stationarity of the wave record D5, the degree of statistical stationarity is plotted for different time windows $\Delta t = 10, 50, 100$ and 300 . It can be observed that with the increase of time window Δt , the DSS index decreases. For each time window, the wave record D5, is high frequency components are more non-stationary than the low frequency. However, the result reveals that highly non-stationary high frequency components can be statistical stationary.

4.4 Linearity

Non-linearity of a particular wave record can be identified by intra-wave frequency modulation which is the fluctuation of instantaneous frequency within one period of oscillation (see [13], [48]). However, to measure non-linearity, degree of non-linearity (DNL) index is introduced by [49]. DNL is proportional to the variance of the instantaneous frequency. Since, large wave amplitude can also contribute towards non-linearity, the degree of non-linearity index (DNL_i) for the i^{th} IMF, can be

defined as (see [25], [26])
$$DNL_i = \text{std} \left\langle \left\{ \frac{\{IF_i - IF_{z_i}\}}{IF_{z_i}} \right\} \cdot \frac{A_{z_i}}{\overline{A_{z_i}}} \right\rangle$$
, where IF being the instantaneous

frequency, IF_z being the full wave zero crossing frequency, A_z being the zero crossing amplitude and $\overline{A_{z_i}}$ is the mean of A_z . On the other hand, the total degree of non-linearity index (TDNL) which is the measure of non-linearity of a wave record having N IMFs, can be defined as (see [25], [26]) ,

$$TDNL = \sum_{i=1}^N \left\langle DNL_j \frac{|C_i|^2}{\sum_{j=1}^N |C_j|^2} \right\rangle, \text{ where } C_i \text{ is the } i^{\text{th}} \text{ IMF.}$$

Table 2. Degree of Non-linearity (DNL) and Total Degree of Non-linearity (TDNL) for the wave record D5.

	IMF1	IMF2	IMF3	IMF4	IMF5	IMF6	IMF7	IMF8
DNL	1.27	0.59	0.65	0.53	1.25	0.61	0.25	0.92
TDNL	0.79							

In Table 2, DNL and TDNL is computed for wave record D5. It can be observed that, DNL is maximum for IMF1 while minimum for IMF7. In the present work, the threshold for non-linear source detection is considered 0.1 (as in [25]). Since all DNL_i s and TDNL are greater than 0.1, non-linear sources are detected in all IMFs and original wave record D5.

To identify phase coupling and non-linear interactions of the wave record, wavelet bicoherence is computed. When the bicoherence closes to 1, three frequencies f_1 , f_2 and f simultaneously present in the wave data and satisfy $f_1 + f_2 = f$ (see [18, 19, 20]). Wavelet bicoherence of the time series D1, D3, D5 and D7 are computed and plotted in Figure 12, to measure phase coupling between dominant IMF (S_1) and sum of the rest IMFs (S_2). In all the figures, at frequencies less than $2^{0.04}$ Hz (0.04 Hz in log 2 scale), the wave interactions are highly non-linear. The figure reveals that, the non-linear interaction is higher at after storm record (D7) than the before storm record (D3) although the group energy and significant wave height is higher in D3 compare to D5. The variations of significant wave heights, mean wave period, time group length and group energy of those time series are shown in Figure 13(a).

4.5 Wave groups

In Table 3, the mean time group length and associated group energy for each selected wave record are shown. To show the accuracy of the energy captured, variance of original data and sum of the total variance are calculated and their differences are shown. It can be observed that the mean group energy increases or decreases with the data variance. The table reveals that mean group energy increases during wave growth and then decreases in post-storm period. However, the wave energy remains higher in the post-storm stage than the pre-storm stage, which agrees with the observation reported by [36]. The largest mean time group length is observed for D3 whilst the smallest for D1. It is important to note that the error difference can be used as a measure of orthogonality. The table also reveals that for the two records D1 and D7, the variance difference error is less than 1%. D2, D5 and D6 show more than 7% error while the rest of the records shows less than 5% error. During the storm, the error is maximum, which may be due to the complex sea states.

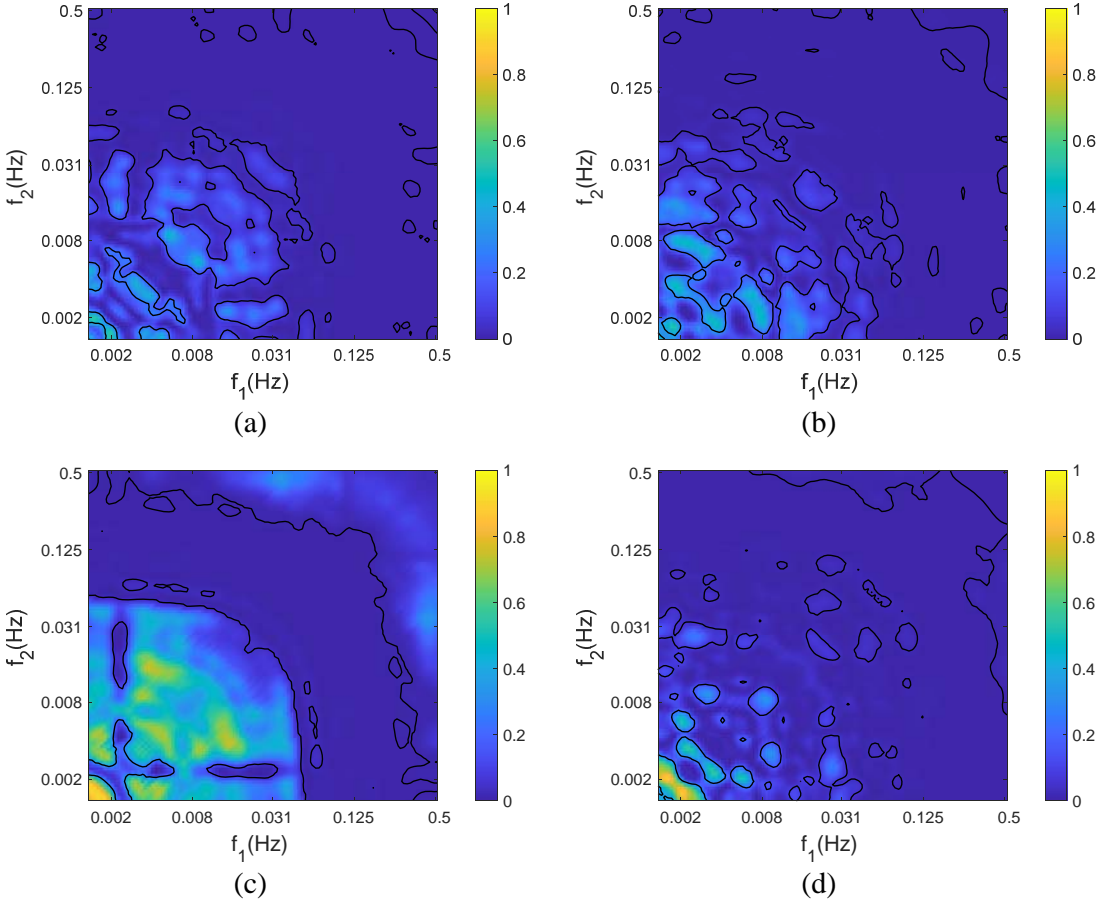


Figure 12. The wavelet bicoherence (phase coupling and non-linear interaction) for wave records (a) D1, (b) D3, (c) D5 and (d) D7.

Table 3. Mean time group length (t_{mgl} (s)), mean group energy (E_{mgr} (m^2)) and comparisons of variance of the original wave record with the sum of IMFs' variances for D1-D8.

	D1	D2	D3	D4	D5	D6	D7	D8
t_{mgl} (s)	43.87	51.58	106.98	59.40	85.57	47.22	52.09	48.66
E_{mgr} (m^2)	30.54	99.06	346.26	338.20	979.99	402.24	120.53	73.17
Data Var. (m^2)	0.260	0.66	1.18	2.08	3.72	2.49	0.87	0.51
Total IMF Var. (m^2)	0.261	0.71	1.24	2.17	4.31	2.75	0.88	0.53
Error in Var. (%)	0.26	7.06	4.72	4.46	15.84	10.27	0.74	4.46

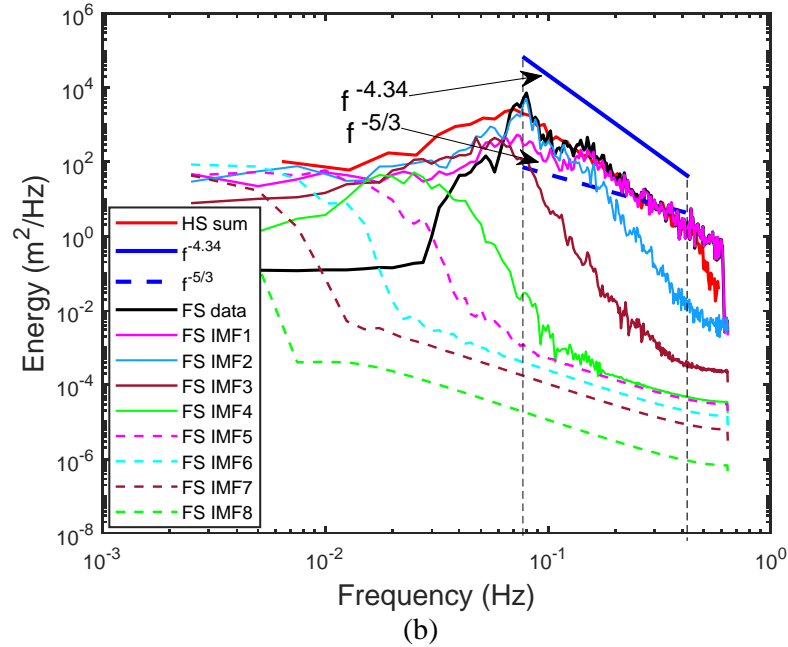
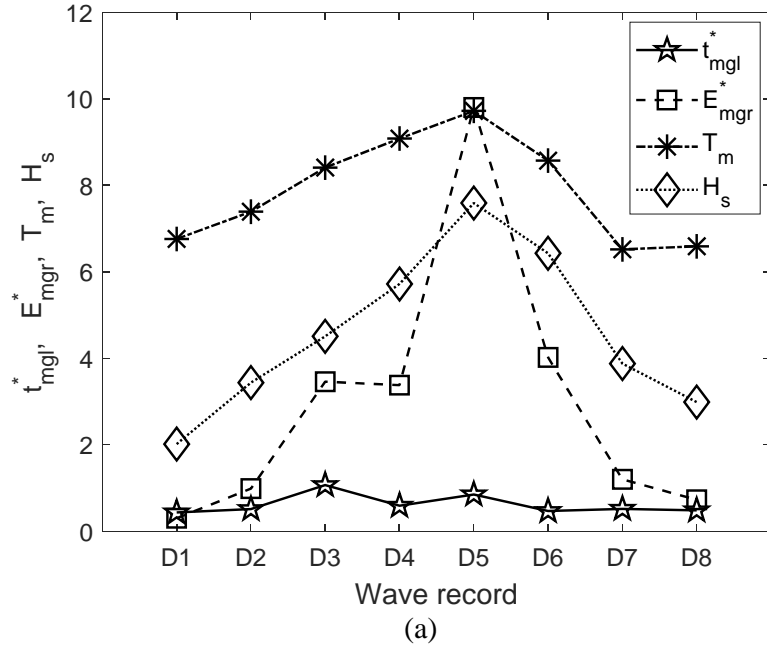


Figure 13. (a) The wave characteristics of different wave records and (b) comparison of Hilbert marginal spectrum (HS sum) with Fourier Spectra for original Data (FS Data) and IMFs for D5.

In Figure 13(a), the variation of significant wave height, mean wave period, time group length and group energy are plotted. In the figure $t_{mgl}^* = 0.01t_{mgl}$ and $E_{mgr}^* = 0.01E_{mgr}$. At calm stage, mean wave period is less than 7s and significant wave height is less than 3m. Then due to the effect of strong wind, the wave growth stage can be observed in the next three measurements with significant wave

height greater than 3m with a shorter wave period. In the wave record D5, the highest significant wave height, mean wave period and group energy are observed. In the wave decay stage, it can be observed that significant wave height and wave period decrease. In post-storm condition, wave becomes smaller in amplitude but longer in periods. In the calm stage, smaller mean time group length observed. Maximum time group length is observed in D3-D5. In Figure 13(b), both the Fourier spectra and the Hilbert spectra of the original data D5, are compared. Fourier marginal spectra of the IMFs are also plotted. There is little similarity between these two kinds of spectrum. The physical interpretation of the energy distribution of both Fourier and Hilbert spectra are different. In Fourier spectrum, energy at a given frequency leads to the existence of trigonometric wave component in the whole time span of the record whilst in marginal Hilbert spectra, for a given frequency, there is a higher likelihood that the energy appears locally. It can be observed that different IMFs present different amount of energy. It is observed that at lower frequency, the Hilbert spectrum dominates Fourier spectrum. It is important to note that the marginal Hilbert spectrum is concentrated around Fourier central frequency. The peak of the IMF spectrum shifts to the left with the increase of IMF's index number. Higher index IMFs contribute smaller energy in the lower frequency range. Most energetic IMFs 1-3 are at the central part of the spectrum. IMF 2 captures most of the energy and its peak frequency coincides with the Fourier spectrum of the original data. In Figure 13(b), slope lines $f^{-\alpha}$ are plotted. It can be observed that, for high frequency within the dashed vertical line, HS sum can be nearly scaled with $f^{-\alpha}$ where $\alpha = 4.34$ (blue solid line) while the slope line $f^{-\alpha}$ where $\alpha = 5/3$ (blue solid line) runs almost parallel with IMF 6, 7 and 8.

5. Conclusions

In the present study, the Hilbert-Huang transformation (HHT) is used for the spectral analysis of wavefield under tropical cyclone Hudhud that took place in October 2014. Different empirical mode decomposition methods, namely EMD, EEMD and CEEMD are compared. It is found that the energy distribution among different intrinsic mode functions (IMFs) is different. In the case of EMD, IMF2 captures maximum energy, while IMF 2 and IMF 4 are most dominant in the cases of EEMD and CEEMD. To measure stationarity and linearity, degree of stationarity (DS), degree of statistical stationarity (DSS), degree of non-linearity and wavelet biocoherence are computed. It is found that Significant wave height's influence on time group length. Group energy is analyzed during different sea stages. The wave energy remains higher in the post-storm stage than in the pre-storm stage. However, the study reveals that during peak cyclone period, the variance difference error is more than 10% due to the complex sea state. Hilbert Marginal Spectra and the Fourier Spectra for the

original record and the corresponding IMFs are compared. It is observed that IMF 2's peak frequency coincides with the Fourier spectrum of the original data.

Acknowledgments

The authors acknowledge the financial support given by the Council of Scientific & Industrial Research, New Delhi and Earth System Science Organization (ESSO)-Indian National Centre for Ocean Information Services (INCOIS), Ministry of Earth Sciences, Government of India to conduct this research. Director, CSIR-National Institute of Oceanography, Goa, and Director, INCOIS for the encouragement provided to carry out the study. We thank officials of INCOIS, Gangavaram Port and Andhra University for the help during the measurement. This is NIO contribution ----.

References

- [1] Balaguru, K., Taraphdar, S., Leung, L.R., Foltz, G.R., Increase in the intensity of postmonsoon Bay of Bengal tropical cyclones, *Geophysical Research Letters* 41 (2014) 3594-3601.
- [2] Barber, N.F. and Ursell, F., The generation and propagation of ocean waves and swell. I. Wave periods and velocities. *Philosophical Transactions of the Royal Society of London. Series A, Mathematical and Physical Sciences*, 240(824) (1948) 527-560.
- [3] Young, I.R., Directional spectra of hurricane wind waves. *Journal of Geophysical Research: Oceans* 111(C8) (2006) C08020.
- [4] Kumar, B.P. and Stone, G.W., Numerical simulation of typhoon wind forcing in the Korean seas using a spectral wave model. *Journal of Coastal Research* 232 (2007) 362-373.
- [5] Xu, F., Perrie, W., Toulany, B. and Smith, P.C., Wind-generated waves in Hurricane Juan. *Ocean Modelling* 16(3-4) (2007) 188-205.
- [6] Chu, P.C. and Cheng, K.F., South China Sea wave characteristics during Typhoon Muifa passage in winter 2004. *Journal of Oceanography* 64(1) (2008) 1-21.
- [7] Soomere, T., Behrens, A., Tuomi, L. and Nielsen, J.W., Wave conditions in the Baltic Proper and in the Gulf of Finland during windstorm Gudrun. *Natural Hazards and Earth System Science* (2008) 37-46.
- [8] Fan, Y., Ginis, I., Hara, T., Wright, C.W. and Walsh, E.J., Numerical simulations and observations of surface wave fields under an extreme tropical cyclone. *Journal of Physical Oceanography* 39(9) (2009) 2097-2116.
- [9] Babanin, A.V., Hsu, T.W., Roland, A., Ou, S.H., Doong, D.J. and Kao, C.C., Spectral wave modelling of Typhoon Krosa. *Natural Hazards and Earth System Sciences* 11(2) (2011) 501-511.
- [10] Amrutha, M.M., Kumar, V.S., Anoop, T.R., Nair, B., Nherakkol, A. and Jeyakumar, C., Waves off Gopalpur, northern Bay of Bengal during cyclone Phailin. *Annales Geophysicae* 32(9) (2014) 1073-1083.

- [11] Rajesh, G., Jossia Joseph, K., Harikrishnan, M. and Premkumar, K. Observations on extreme meteorological and oceanographic parameters in Indian seas. *Curr. Sci* 88(8) (2005) 1279-1282.
- [12] Titchmarsh EC. *Introduction to the Theory of Fourier Integrals*. Oxford: Oxford Univ. Press (1948).
- [13] Huang, N.E., Shen, Z., Long, S.R., Wu, M.C., Shih, H.H., Zheng, Q., Yen, N.C., Tung, C.C. and Liu, H.H., The empirical mode decomposition and the Hilbert spectrum for nonlinear and non-stationary time series analysis. *Proceedings of the Royal Society of London. Series A: Mathematical, Physical and Engineering Sciences* 454 (1998) 903-995.
- [14] Mandic, D. P., Rehman, N., Wu, Z., and Huang, N. E., Empirical mode decomposition-based time-frequency analysis of multivariate signals: The power of adaptive data analysis. *IEEE signal processing magazine*, 30(6) (2013) 74-86.
- [15] Boashash, B., Estimating and interpreting the instantaneous frequency of a signal. I. Fundamentals. *Proceedings of the IEEE*, 80(4) (1992) 520-538.
- [16] Singh, P., Joshi, S.D., Patney, R. K., and Saha, K., The Fourier decomposition method for nonlinear and non-stationary time series analysis. *Proceedings of the Royal Society A: Mathematical, Physical and Engineering Sciences*, 473(2199) (2017) 20160871.
- [17] Choudhury, M.S., Shah, S.L., and Thornhill, N. F., Diagnosis of poor control-loop performance using higher-order statistics. *Automatica*, 40(10), (2004) 1719-1728.
- [18] Elsayed, M. A., Wavelet bicoherence analysis of wind-wave interaction. *Ocean Engineering*, 33(3-4) (2006) 458-470.
- [19] Dong, G., Ma, Y., Perlin, M., Ma, X., Yu, B., and Xu, J., Experimental study of wave-wave nonlinear interactions using the wavelet-based bicoherence. *Coastal Engineering*, 55(9) (2008) 741-752.
- [20] Ma, Y., Dong, G., Liu, S., Zang, J., Li, J., and Sun, Y., Laboratory study of unidirectional focusing waves in intermediate depth water. *Journal of engineering mechanics*, 136(1) (2010) 78-90.
- [21] Hasselmann, K., Munk, W., MacDonald, G., Bispectra of ocean waves. In: Rosenblatt, M. (Ed.), *Time Series Analysis*. Wiley, New York, (1963) 125-139.
- [22] Elgar, S., Guza, R. T., Observations of bispectra of shoaling surface gravity waves. *Journal of Fluid Mechanics*, 161 (1985) 425-448.
- [23] Elgar, S., Guza, R. T., and Freilich, M. H., Observations of nonlinear interactions in directionally spread shoaling surface gravity waves. *Journal of Geophysical Research: Oceans*, 98(C11) (1993) 20299-20305.
- [24] Vincent, C., Giebel, G., Pinson, P., and Madsen, H., Resolving nonstationary spectral information in wind speed time series using the Hilbert-Huang transform. *Journal of Applied Meteorology and Climatology*, 49(2) (2010) 253-267.
- [25] Aftab, M. F., Hovd, M., Huang, N. E., and Sivalingam, S., An adaptive non-linearity detection algorithm for process control loops. *IFAC-PapersOnLine*, 49(7) (2016) 1020-1025.

- [26] Aftab, M. F., Hovd, M., and Sivalingam, S., Detecting non-linearity induced oscillations via the dyadic filter bank property of multivariate empirical mode decomposition. *Journal of Process Control*, 60 (2017) 68-81.
- [27] Wu, Z., Huang, N. E., Ensemble empirical mode decomposition: a noise-assisted data analysis method. *Advances in adaptive data analysis*, 1(01) (2009) 1-41.
- [28] Torres, M. E., Colominas, M. A., Schlotthauer, G., and Flandrin, P., A complete ensemble empirical mode decomposition with adaptive noise. *IEEE international conference on acoustics, speech and signal processing (ICASSP)* (2011-May) 4144-4147.
- [29] Huang, N. E., Shen, Z., & Long, S. R., A new view of nonlinear water waves: the Hilbert spectrum. *Annual review of fluid mechanics*, 31(1) (1999) 417-457.
- [30] Huang, N. E., Hilbert-Huang transform and its applications. *World Scientific*, (16) (2014).
- [31] Goda, Y., Numerical experiments on wave statistics with spectral simulation. *Report Port Harbour Res. Inst.* 9 (1970) 3-57.
- [32] Dong, G.H., Ma, Y.X., and Ma, X.Z., Cross-shore variations of wave groupiness by wavelet transform. *Ocean engineering*, 35(7) (2008) 676-684.
- [33] Medina, J.R. and Hudspeth, R.T., A review of the analyses of ocean wave groups. *Coastal Engineering* 14(6) (1990) 515-542.
- [34] Masson, D. and Chandler, P., Wave groups: a closer look at spectral methods. *Coastal Engineering* 20(3-4) (1993) 249-275.
- [35] Liu, P.C., Wavelet transform and new perspective on coastal and ocean engineering data analysis. *Advances in coastal and ocean engineering* 6 (2000) 57-102.
- [36] Veltcheva, A.D., Wave and group transformation by a Hilbert spectrum. *Coastal Engineering Journal* 44(4) (2002) 283-300.
- [37] Schlurmann, T., Spectral analysis of nonlinear water waves based on the Hilbert-Huang transformation. *J. Offshore Mech. Arct. Eng.* 124(1) (2001) 22-27.
- [38] Veltcheva, A.D. and Soares, C.G., Identification of the components of wave spectra by the Hilbert Huang transform method. *Applied Ocean Research* 26(1-2) (2004) 1-12.
- [39] Ortega, J. and Smith, G.H., Hilbert–Huang transform analysis of storm waves. *Applied Ocean Research* 31(3) (2009) 212-219.
- [40] Veltcheva, A. and Soares, C.G., Analysis of wave groups by wave envelope-phase and the Hilbert Huang transform methods. *Applied Ocean Research* 60 (2016) 176-184.
- [41] Anjali Nair, M., Sanil Kumar, V., Amrutha, M.M. and Murty, V.S.N., Features of locally and remotely generated surface gravity waves in the inner-shelf region of north-western Bay of Bengal, *International Journal of Climatology*, 39 (2019) 1644-1664 doi: 10.1002/joc.5907
- [42] Huang, N.E., Shen, Z. and Long, S.R., A new view of nonlinear water waves: the Hilbert spectrum. *Annual review of fluid mechanics* 31(1) (1999) 417-457.

- [43] Huang, N.E., Wu, M.L.C., Long, S.R., Shen, S.S., Qu, W., Gloersen, P. and Fan, K.L., A confidence limit for the empirical mode decomposition and Hilbert spectral analysis. Proceedings of the Royal Society of London. Series A: Mathematical, Physical and Engineering Sciences 459(2037) (2003) 2317-2345.
- [44] Longuet-Higgins, M.S., On the statistical distribution of the height of sea waves. J. Mar. Res., 11 (1952) 245-266.
- [45] Mori, N., Onorato, M., and Janssen, P. A. E. M., On the Estimation of the Kurtosis in Directional Sea States for Freak Wave Forecasting, J. Phys. Oceanogr., 41 (2011) 1484-1497,.
- [46] Anjali, N., Sanil Kumar, V., Growth and decay of wave spectrum during tropical cyclone Hudhud. INCHOE, Indian Society for Hydraulics and Central Water & Power Research Station, Pune, India, (2018).
- [47] Veltcheva, A. D., An application of HHT method to the nearshore sea waves. In The Hilbert–Huang transform in engineering, CRC Press, (2005) 97-119.
- [48] Veltcheva, A., Soares, C. G., Nonlinearity of abnormal waves by the Hilbert–Huang Transform method. Ocean Engineering, 115 (2016) 30-38.
- [49] Huang, N. E., Lo, M.-T., Zhao-Hua W., Xian-Yao C., Method for quantifying and modeling degree of nonlinearity, combined nonlinearity, and nonstationarity, US Patent 8,732,113 (2014).